JOURNAL OF THERMOPHYSICS AND HEAT TRANSFER
Vol. 15, No. 2, April–June 2001

Effect of Void-Generated Thermocapillary Convection on Dopant Segregation in Microgravity Solidification

M. Kassemi*
NASA John H. Glenn Research Center at Lewis Field, Cleveland, Ohio 44135
and
M. Kaforey† and D. Matthiesen‡
Case Western Reserve University, Cleveland, Ohio 44106

Three recent microgravity experiments have been hampered by convection caused by unwanted voids and/or bubbles in the melt. We present a numerical study to delineate the influence of void-generated thermocapillary convection on solidification of a doped single crystal from its dilute binary melt in microgravity. A detailed numerical model for the Bridgman solidification process is developed. The finite element numerical model solves the quasi-steady Navier–Stokes equations, together with the conservation equations for transport of energy and species. The complicating effects of thermocapillary convection generated by the void and solutal rejection at the melt–solid interface are included. Through a quasi-steady analysis, it is shown that the convection generated by the void can affect radial segregation drastically, especially if the thermocapillary vortex penetrates the solutal boundary layer at the growth interface. From a transport point of view, three different regimes are identified based on the distance between the void and the growth interface. These range from a diffusion-controlled regime, where most of the radial nonuniformity in the interfacial composition is due to interface curvature with minimal flow effects, to a fully mixed regime, where the penetration of the solutal boundary layer by the thermocapillary vortex tends to homogenize the interfacial compositions.

Nomenclature

C = scaled concentration, C^*/C_0
Ca = capillary number, $\gamma_T \Delta T_b/\gamma = \mu U_0/\gamma$
C_0 = bulk dilute concentration
C^* = concentration
c_p = specific heat, J/kg °C
D = diffusion coefficient
Gr = Grashof number, $g\beta R^3 \Delta T/\nu^2$
$\boldsymbol{g}$ = gravitational vector, $g_0 \hat{e}_g$, m/s^2
g_0 = Earth's gravitational acceleration, 9.8 m/s^2
H = mean Gaussian curvature parameter, 1/m
k = thermal conductivity, W/m °C
k_p = partition coefficient
L = height of the melt region, m
L_{hg} = height of the steep gradient region, m
l = void–interface distance, m
Ma = Marangoni number, $Re \cdot Pr$
$\hat{\boldsymbol{n}}$ = unit normal vector
P = pressure, N/m^2
Pr = Prandtl number, ν/α
R = crucible radius, m
R_b = void radius, m
Re = Reynolds number, $U_0 R_b/\upsilon$
r = radial coordinate, m
Sc = Schmidt number, ν/D
T = temperature, °C
U_p = crystal pulling velocity, m/s
U_0 = characteristic thermocapillary velocity, $\gamma_T \Delta T_b/\mu\nu$, m/s
u = axial velocity component, m/s
$\boldsymbol{V}$ = velocity vector, m/s
v = radial velocity component, m/s
z = axial coordinate, m
β = thermal expansion coefficient, 1/°C
γ = surface tension, kg/s^2
γ_T = thermal coefficient of surface tension, kg/s$^2 \cdot$ °C
ΔT = $T_h - T_m$
ΔT_b = nominal temperature difference between the top and bottom of the void
μ = dynamic viscosity, kg/m · s
ν = kinematic viscosity, m^2/s
ρ = melt density, kg/m^3
ρ_c = solid density, kg/m^3
σ = stress, kg/m · s^2
ψ = stream function, m^2/s

Subscripts

a = bubble pressure
b = void/bubble
c = solid
h = hot
m = melting temperature
n = normal
t = tangential

Introduction

SOLIDIFICATION experiments, especially microgravity solidification experiments, are often compromised by the evolution of unwanted voids or bubbles in the melt. Although these voids and/or bubbles are highly undesirable, there is currently no effective means of preventing their formation or of eliminating their adverse effects, particularly during microgravity experiments. Marangoni convection caused by these voids can drastically change the transport processes in the melt. Recent microgravity experiments by Matthiesen and Majewski,[1] Andrews et al.,[2] and Fripp et al.[3] are perfect examples of the effects of voids and bubbles on the outcome of costly space experiments and significantly increase the level of difficulty in interpreting their results.

Unlike natural convection, which is driven by density differences generated by either temperature or concentration gradients in the

Presented as Paper 2000-0703 at the AIAA 38th Aerospace Sciences Meeting, Reno, NV, 11–13 January 2000; received 25 April 2000; revision received 28 September 2000; accepted for publication 29 September 2000.

*Senior Research Scientist, National Center for Microgravity Research, MS 110-3, 21000 Brook Park Road; Mohammad.Kassemi@grc.nasa.gov.
†Associate Professor, Department of Materials Science.
‡Principal Researcher, Department of Materials Science.

bulk of the melt, void-generated Marangoni convection is driven by surface tension forces brought about by temperature or concentration gradients (thermocapillary and solutocapillary convection, respectively) along the free surfaces of the void or bubble. On Earth, the volumetric forces are dominant, especially in apparatuses with large volume-to-surface ratio. However, in the reduced gravity environment of orbiting spacecraft, surface forces become more important. As a result, the void-generated Marangoni convection can easily alter the flow, temperature, and concentration fields in the melt. Naturally, if these effects are strong enough to extend to the solidification front, they can change interfacial concentration and temperature gradients and lead to unexpected growth conditions. In this work, we will investigate, for the first time, the effects of thermocapillary convection generated by voids and/or bubbles on directional solidification of a single crystal from its dilute binary melt.

Formation of bubbles has caused problems in microgravity experiments for a long time. Even in the early Skylab mission, an unexpectedly large number of bubbles were detected in the four materials processing experiments reported by Papazian and Wilcox.[4] They demonstrated that whereas during ground-based tests bubbles were seen to detach from the interface easily and float to the top of the melt, in low-gravity tests no detachment from the interface occurred and large voids were grown in the crystal.

More recently, the lead–tin–telluride crystal growth experiment of Fripp et al.,[3] flown aboard the United States Microgravity Payload 3 mission, has provided very interesting results. The purpose of the study was to investigate the effect of natural convection on the solidification process by growing the samples at different orientations with respect to the gravitational field. Large pores and voids were found in the three solid crystal samples processed in space. Postgrowth characterization of the compositional profiles of the cells indicated considerable levels of mixing even in the sample grown in the hot-on-top stable configuration. The mixing was attributed to thermocapillary convection caused by the voids and bubbles that evolved during growth. Because the thermocapillary convection is orientation independent, diffusion-controlled growth was not possible in any of the samples, even the top-heated one.

Another microgravity experiment that has reported significant evolution of voids in the melt is the dopant segregation study of Matthiesen and Majewski,[1] which involved solidification of selenium-doped GaAs in microgravity during the United States Microgravity Laboratory 1 (USML-1) mission. The experiment was designed to investigate the effects of the microgravity environment, the translation rate, and the furnace thermal profile on the axial and radial dopant distributions. Two samples were solidified, both of which contained a considerable number of voids. Both samples also exhibited concentrations that were more uniform than expected, especially in the region right below the voids. Moreover, postgrowth measurements of the selenium dopant concentration in the sample indicated a behavior that could not be easily deciphered. This again suggested the possibility that the diffusion-controlled growth conditions were disrupted by vigorous mixing attributed to surface tension-driven convection generated by the voids.

Voids were also present in the microgravity Al–In alloy solidification experiment carried out by Andrews et al.,[2] which flew aboard the Life and Microgravity Spacelab mission in the summer of 1996. The goal of the microgravity research was to control growth conditions in the absence of buoyancy-driven convection. To promote stable interfacial conditions, a steep thermal gradient of 100°C/cm was required in the sample. All three processed samples contained a considerable number of voids, which were attributed to sticking pistons and entrapped gases liberated during the process. Because it was not possible to control the temperature gradient in the samples effectively, the gradients in all three samples were considerably lower than necessary to promote interface stability. Once again, there was incredible difficulty in interpreting the results of this experiment.

Finally, two experiments have directly investigated thermocapillary convection generated by voids/bubbles in reduced gravity using silicone oil as a model fluid. The first microgravity experiment, undertaken by Naumann,[5] flew on the USML-1 mission in 1992. The second is the reduced gravity experiments of Wozniak et al.[6] aboard the European TEXUS 33 sounding rocket. The results of these experiments clearly indicate that flows induced by thermocapillary convection can be at least three orders of magnitude larger than the buoyancy-driven convective flows caused by residual acceleration. The aforementioned studies, however, both involve model fluids without any phase change. Therefore, they do not directly address the impact of void-generated thermocapillary convection on alloy solidification in microgravity.

These results are all consistent with recent studies of thermocapillary convection generated by a bubble on a heated surface performed by Kassemi and Rashidnia[7,8] and Kassemi et al.,[9] where it is numerically and experimentally shown that the thermocapillary flow generated by a bubble can drastically modify the temperature field through vigorous mixing of the fluid around it, especially under microgravity conditions.

In this paper we will consider the effect of thermocapillary convection generated by a void/bubble on the growth of a typical single crystal alloy in microgravity. In particular, we will examine, in detail and for the first time, the manner in which the void-generated convection can modify the temperature stratification and the segregation patterns in the dilute binary melt during various stages of a microgravity solidification experiment. We will also quantify and underscore the serious impact of void and bubbles on the interfacial composition during the growth of the doped crystal.

Mathematical Formulation

Consider the growth of a single crystal (in this case, selenium-doped GaAs) from a dilute two-component melt in a vertical Bridgman furnace as depicted in Fig. 1 and Tables 1 and 2. This configuration is similar to the one used in Matthiesen and Majewski's segregation experiment[1] aboard the 1996 USML-1 mission, where large and small voids were present in the melt during the entire solidification process. The ampoule is placed in a three-zone furnace that consists of a shallow gradient hot zone separated from a constant temperature cold zone by a sharp gradient region. Directional solidification takes place as the ampoule is translated at a constant rate. The transport of heat among the solid, the melt, the ampoule, and the furnace determines the solid–melt interface shape and position.

Because the crystal pulling velocity is small (for the cases considered here) and the ampoule is sufficiently long, a quasi-steady analysis is justified, and the effects of latent heat of fusion can be

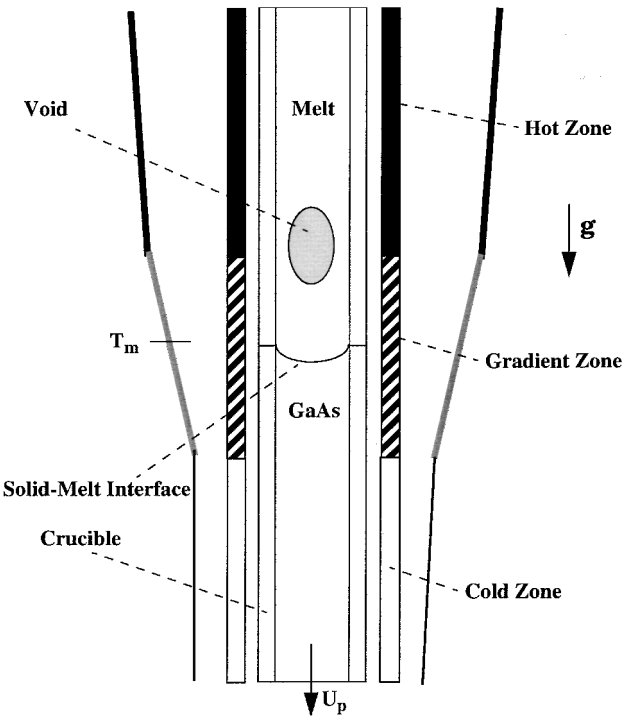

Fig. 1 Schematic of the Bridgman growth configuration.

Table 1 Thermophysical properties and growth parameters for selenium-doped GaAs

Parameter	Value
Dynamic viscosity	0.0043 kg/m · s
Thermal conductivity	17.77 W/m · s °C
Density	5720 kg/m^3
Volume expansion	$1.87(10)^{-5}$ °C^{-1}
Surface tension at T_m	0.482 kg/s^2
Thermal coefficient of surface tension	$-0.96(10)^{-3}$ kg/s^2 °C
Specific heat capacity	434.7 J/kg °C
Partition coefficient	0.10
Diffusion coefficient	$2(10)^{-9}$ m^2/s
Growth rate	$1.66(10)^{-6}$ m/s
T_m	1238°C
T_h	1260°C
L_{hg}	0.03 m
Steep gradient	733°C/m
Hot zone gradient	34.8°C/m
Void radius	0.0044 m

Table 2 Dimensionless parameters

Parameter	Value
Pr	0.1
Sc	375
Gr	0.004
Re[a]	400–8450
Ca[a]	0.00062–0.014

[a]Values correspond to the void in high and low temperature gradient regions.

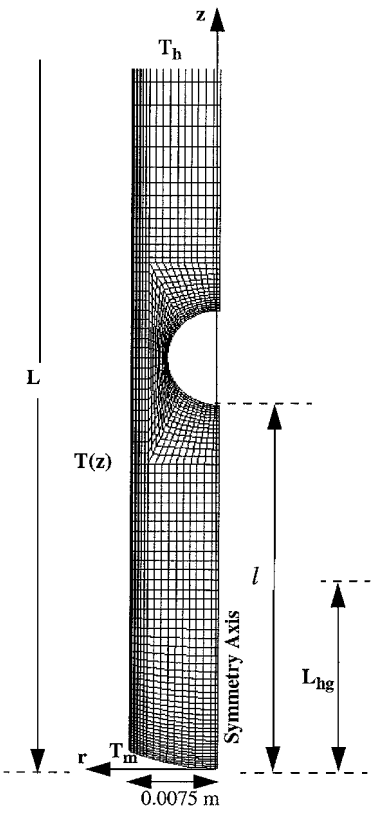

Fig. 2 Finite element mesh for melt region (only lower section of mesh shown).

neglected. Therefore, it is possible to restrict the present analysis to the melt region alone, as shown in Fig. 2. In the actual Bridgman growth system, the solidification interface is inherently curved due to the mismatch between the thermal conductivities of the melt, the solid, and the thick-walled crucible and due to the heat transfer coupling between the ampoule and the furnace. The curvature and position of the solid–liquid interface are very important because they can affect the compositional nonuniformity near the growth interface. Therefore, the nonplanar shape and the position of the interface as dictated by the furnace–crucible heat transfer link are extracted from the experimental results[1] and used to define the melt region as shown in Fig. 2. It is also assumed that the longitudinal axis of the ampoule is aligned with the net gravitational vector. Therefore, the bore temperature profiles established by the furnace are circumferentially uniform, and axisymmetric conditions can be exploited.

When a void is present in the melt, surface tension forces created by the temperature gradient along the melt–void interface will drive a strong thermocapillary flow. In microgravity and under the top-heated growth configuration adopted here, the thermocapillary convection is the main driver of the flow and disrupts the thermal and solutal stratification in the ampoule, resulting in significant alteration of the temperature and compositional profiles near the melt–solid interface. The thermocapillary convection generated by the bubble also implies that the bubble will be moving in the melt toward the hot end. In this analysis, our goal is to show the effect of thermocapillary convection on the solidification process as a function of the relative position of the void with respect to the growth interface. Therefore, with the quasi-steady approach, the locations of the void and the solidification front are fixed in each simulation, but the distance between the void and the solidification front is varied in a series of quasi-steady simulations to show the impact of the thermocapillary convection during different stages of the solidification process.

Following the quasi-steady formulations, a two-dimensional axisymmetric model is developed to describe the fluid flow and heat and mass transport induced by the void in the melt. In this work, the Boussinesq approximation is used to represent the density gradients in the buoyancy term, which is valid for small temperature differences. All of the material properties, except for the surface tension coefficient, are assumed to be constant. The dependence of surface tension on temperature is incorporated into the model using the measurements performed by Shetty et al.[10] Translation of the ampoule is modeled by supplying a doped melt of a dilute bulk composition C_0 at a constant velocity U_p at the top of the melt region and withdrawing a solid of composition C from the bottom. The interface is at T_m, the melting temperature of the crystal, whereas the upper boundary is held at a higher temperature T_h. The longitudinal temperature $T(z)$ prescribed by the furnace is applied at the side.

The flow in the enclosure is described by the continuity and momentum equations, which are written as

$$\nabla \cdot \boldsymbol{V} = 0 \tag{1}$$

$$\rho_m(\boldsymbol{V} \cdot \nabla \boldsymbol{V}) = -\nabla P + \mu \nabla^2 V + \rho_m \boldsymbol{g} - \rho_m \boldsymbol{g} \beta (T - T_m) \tag{2}$$

These equations are subject to the solidification velocity condition at the top, bottom, and side boundaries

$$u = U_p(\rho_c/\rho_m), \qquad v = 0 \tag{3}$$

and symmetry conditions along the central axis of the enclosure and normal and tangential stress balances along the surface of the bubble

$$\sigma_n = 2\gamma H - P_a \tag{4}$$

$$\sigma_t = \gamma_T \nabla_t T \tag{5}$$

Note that there are two driving forces for the flow. The first is due to the surface tension force, which drives a vigorous tangential velocity along the void surface. The second is the buoyancy force, which is driven by the density differences in the bulk of the fluid. Because both surface tension and density are functions of temperature, both of these driving forces couple the momentum equation to the energy equation. The energy equation is written as

$$\rho_m c_p(\boldsymbol{V} \cdot \nabla T) = k \nabla^2 T \tag{6}$$

This equation is subject to symmetry condition at the centerline and prescribed temperatures at the top, bottom, and sidewalls, respectively.

The top is

$$T = T_h \tag{7}$$

The solid–melt interface is

$$T = T_m \tag{8}$$

The side is

$$T = T_\infty(z) \tag{9}$$

The segregation behavior in the melt is governed by the conservation of species equation, which is written as

$$\rho_m(\boldsymbol{V} \cdot \nabla C) = \rho_m D \nabla^2 C \tag{10}$$

This equation is subject to the following boundary conditions: The top is

$$\rho_m D(\hat{n}_z \cdot \nabla C) = \rho_s U_p(C - 1) \tag{11}$$

The solid–melt interface is

$$\rho_m D(\hat{n}_z \cdot \nabla C) = \rho_s U_p(1 - k_p)C \tag{12}$$

The side and centerline are

$$(\hat{n}_r \cdot \nabla C) = 0 \tag{13}$$

Finally, note that in formulating the present model, it is inherently assumed that the vapor in the bubble is not in thermodynamic equilibrium with the melt. If thermodynamic equilibrium prevails, then the interface assumes a temperature close to the saturation temperature and the temperature gradient along the interface will be greatly relaxed. Moreover, the effects of radiation exchange between the enclosed surfaces of the void, which will also tend to reduce the temperature gradients along the interface, are also neglected. This is a fair assumption because the conductive and convective contributions of the highly conductive semiconductor melt to the interfacial energy balance can easily dominate the conduction/radiation heat transfer inside the void. In any case, both the thermodynamic equilibrium and the radiation effects tend to minimize the thermocapillary convection, and so the results generated here can be regarded as the worst-case scenario as far as the extent of the thermocapillary convection is concerned.

Numerical Solutions

To solve the problem numerically, a finite element model for the problem is developed. In this two-dimensional axisymmetric model, the void is treated as a flexible free surface. The shape of the void–melt interface is an unknown variable that is updated as the solution evolves. The boundary conditions on the void–melt interface [Eqs. (4) and (5)] are written as continuities of normal and tangential stresses and the kinematic constraint that requires the interface to always remain an interface. When this scheme is used, which is sometimes referred to as kinematic updating, the balance of tangential and normal stresses is used to satisfy the boundary conditions for the momentum equation, and the kinematic constraint is used to determine the position of the void–melt interface. Consequently, as the solution progresses, the positions of all of the nodes are adjusted according to the updated position of the interface.

As mentioned earlier, the solid–melt interface is assumed to be fixed in this quasi-steady analysis, and its shape is assumed to be dictated by the furnace crucible configuration. The position of the void is also fixed by setting the velocities at the void tips on the symmetry line equal to zero and fixing the contact angle between the void free surface and the symmetry axis to be 90 deg. The void is still modeled as a deformable surface as mentioned before, but because the Ca for the cases considered here is quite small (0.014 in the high gradient region and 0.0006 in the low gradient region), the flow has basically no effect on the shape of the void, and it remains essentially spherical.

The system of coupled simultaneous nonlinear equations is solved using a nominally quadratic quasi-Newton algorithm. Two convergence criteria must be simultaneously satisfied to arrive at the final solution. These are

$$\|(S_i - S_{i-1})/S_i\| \leq \text{STOL} \tag{14}$$

$$\|F_i/F_0\| \leq \text{FTOL} \tag{15}$$

where S_i and F_i are respectively the solution and residual force vectors at iteration i. The norm $\|\|$ is a root mean square norm summed over all of the equations and solution tolerance (STOL) and forcing function tolerance (FTOL) were set to be 0.00001 and 0.0001, respectively.

Each of the quasi-steady calculations was started from a motionless state with a uniform concentration field at C_0 and the thermal field in conductive equilibrium. Sensitivity of the final solution to the initial guessed conditions was checked by also starting some solutions using the results of already converged nearby parameter cases. Identical solutions were found in all test cases.

The solutions presented in this paper are generated using 2820 nine-node quadratic elements (10,301 nodes) with dense clustering of the nodes near the solid–melt and void–melt interfaces to resolve the very thin solutal and momentum boundary layers that form at these boundaries, respectively. Grid resolution independence was checked by comparing solutions generated by three coarser grids (with 1980, 1504, and 768 elements) with solutions on the finest mesh. Examples of the grid resolution results based on temperatures of a point on the surface of the bubble, the maximum velocity, the minimum stream function, and the maximum and minimum interfacial concentrations are presented in Tables 3 and 4 for two different void–interface distances. In Tables 3 and 4, the quantities in parentheses represent the difference between predictions of the coarser grids and those of the finest grid. The comparisons indicate excellent grid resolution for all designated test variables.

The numerical code was further validated by comparing temperature and velocity fields and bubble shapes with limiting benchmark

Table 3 Grid convergence results for $l = 0.0195$ m

Grid size (elements)	Maximum velocity, m/s	Maximum stream function, m^2/s	Maximum interfacial concentration	Minimum interfacial concentration	Temperature at point P, °C
768	0.05335 (4%)	−0.007754 (0.4%)	1.2689 (0.03%)	1.0550 (1.1%)	1256 (0%)
1504	0.05401 (2.8%)	−0.007739 (0.6%)	1.2687 (0.015%)	1.0624 (0.4%)	1256 (0%)
1980	0.05512 (0.8%)	−0.007775 (0.12%)	1.2687 (0.015%)	1.0665 (0.02%)	1256 (0%)
2820	0.05557	−0.007785	1.2685	1.0668	1256

Table 4 Grid convergence results for $l = 0.032$ m

Grid size (elements)	Maximum velocity, m/s	Minimum stream function, m^2/s	Maximum interfacial concentration	Minimum interfacial concentration	Temperature at point P, °C
768	0.01657 (4.5%)	−0.001904 (0.4%)	1.9489 (2%)	1.4065 (3%)	1260 (0%)
1504	0.01683 (3%)	−0.001902 (0.5%)	1.9298 (1%)	1.3792 (1%)	1260 (0%)
1980	0.01718 (1%)	−0.001910 (0.1%)	1.9202 (0.5%)	1.3723 (0.5%)	1260 (0%)
2820	0.01735	−0.001912	1.9107	1.3655	1260

results of an air bubble subject to a temperature gradient in a model fluid (silicone oil) medium. The validations includes the following: 1) comparison with published experimental results for both ground-based and microgravity measurements,[6] 2) comparison with published numerical results for both ground-based and microgravity measurements,[7,8] and 3) comparison of numerically predicted index of refraction gradient fringe patterns with experimentally measured Wollaston prism interferograms obtained in our laboratory for both steady-state and transient cases.[9] The agreements were excellent for all cases as described by Kassemi and Rashidnia.[11]

Results and Discussion

All of the cases examined in this section are based on growth of selenium-doped GaAs in a top-heated Bridgman furnace configuration under microgravity conditions ($g = 10^{-6} g_0$). The dimensions, growth conditions, and material properties, which were used to generate the numerical simulations, are very similar to the ones used in Matthiesen and Majewski's segregation experiment[1] and are included in Figs. 1 and 2 and in Tables 1 and 2. The two-component system considered consists of GaAs as a single entity with the dopant selenium, at dilute concentrations, as the solute. The partition coefficient for selenium is given in Table 1, and the values of some of the relevant dimensionless numbers governing the transport processes in the melt are included in Table 2. In the experiment in Ref. 12, several jointed oblong-shaped bubbles were present. In the model, these voids are represented by a single spherical void with a volume equivalent to the sum of the void volumes in the actual experiment. In this section, the effect of thermocapillary convection generated by the void on interfacial segregation patterns will be demonstrated through a series of simulations that, following the quasi-steady approach, can be regarded as snapshots in time as the distance between the interface and the void varies during the solidification process. Each solution is generated by a quasi-steady simulation in which the distance between the void and the melt interface is fixed at a specified value.

The first case that we consider corresponds to the reference situation, where there are no voids in the melt. The temperature, flow, and dopant concentration fields for the melt with a flat interface are included in Fig. 3, and the temperature, flow, and dopant concentration fields for a melt with a curved growth interface (shape extracted from the corresponding experimental results[1]) are shown in Fig. 4. All isocontours presented are equally spaced between the minimum and maximum values for each case. Both cases show buildup of the rejected solute near the growth interface. However, note the following. First, in the absence of voids and under microgravity conditions, the flow in the ampoule is mainly due to the solidification process. This flow is very weak and uniform due to the small pulling velocity. Therefore, the resultant temperature and concentration fields shown in Figs. 3 and 4 correspond to a diffusion-controlled state. Second, the interfacial concentration profiles shown in Fig. 5 indicate that, although the radial concentration profile for the flat interface is very uniform, the radial concentration profile for the curved interface is highly parabolic, with an accumulation of dopant near the middle of the curved interface (see also Fig. 4). This implies that, as others have reported,[13] the shape of the interface has a considerable impact on the radial segregation. Thus, the curved interface shape extracted from the microgravity experiment[1] will be retained in all of the case studies presented in this section.

The next cases we consider correspond to a situation where a void is present in the melt. Quasi-steady simulations show the effect of the thermocapillary convection generated by the void on the temperature and concentration fields in the melt at different stages of the solidification process as the solid–melt interface approaches the void.

The first case examined corresponds to a stage of the solidification process where there is a relatively large distance between the growth interface and the void ($l = 0.0456$ m). The axial concentration profile (at the center of the ampoule) for this case is presented in Fig. 6, and the temperature, concentration, and flowfields are presented in Fig. 7. In this situation, the void is in the shallow gradient region (hot zone) of the ampoule. Nevertheless, a thermocapillary vortex

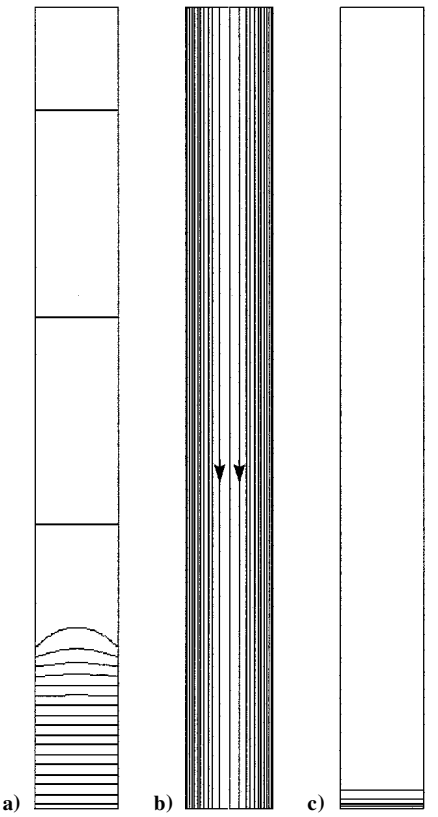

Fig. 3 Flat interface case: a) temperature field (20 contours, T_{min} = 1238°C and T_{max} = 1264°C), b) streamlines [10 contours, ψ_{min} = $-0.29(10)^{-5}$ m²/s, ψ_{max} = 0], and c) concentration field (5 contours, C_{min} = 1.0 and C_{max} = 10).

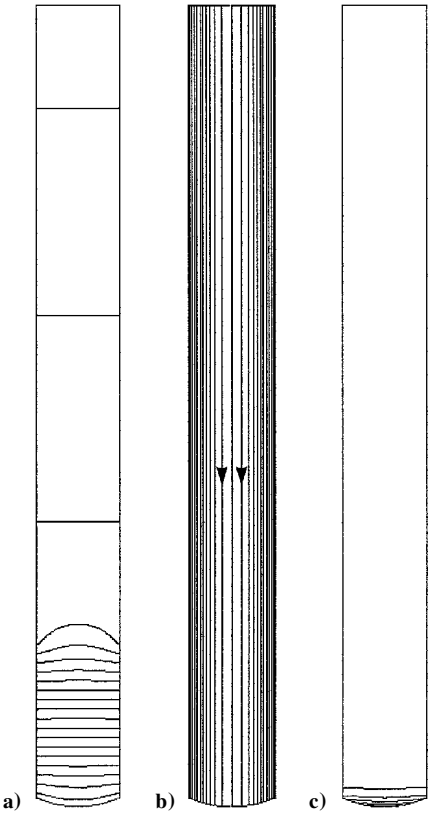

Fig. 4 Curved interface case: a) temperature field (20 contours, T_{min} = 1238°C and T_{max} = 1264°C), b) streamlines [10 contours, ψ_{min} = $-0.29(10)^{-5}$ m²/s, ψ_{max} = 0], and c) concentration field (5 contours, C_{min} = 1.0 and C_{max} = 21.59).

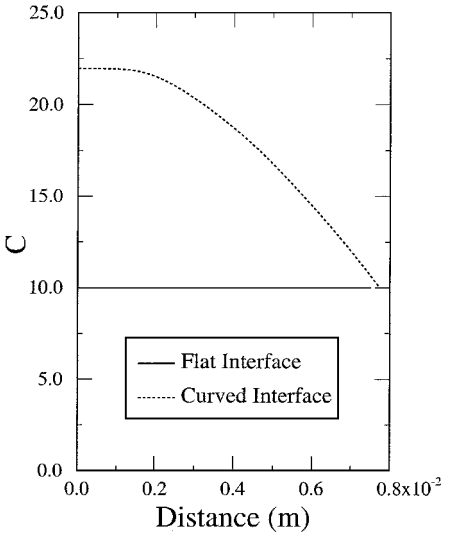

Fig. 5 Concentration as a function of the distance along the solid–melt interface for the flat and curved interface cases.

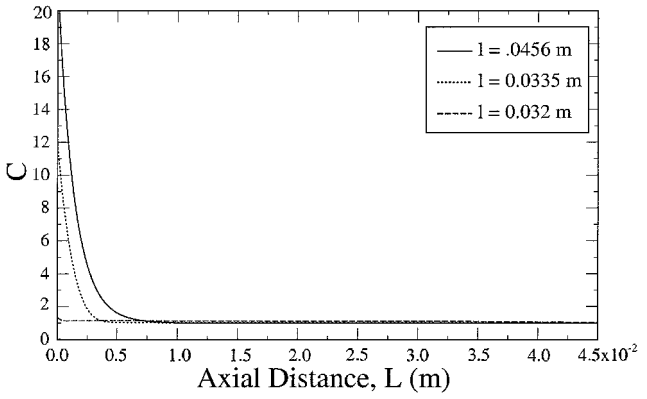

Fig. 6 Concentration along the central axis of symmetry for different void–interface distances.

is generated in the vicinity of the bubble, as shown in Fig. 7b. The vortex recirculates the fluid along the void interface in a clockwise direction (refers to the left half of the toroidal circulation). The flow is not too strong (Fig. 8) and is restricted to the mostly uniform temperature and concentration regions of the ampoule; therefore, it does not affect the melt temperature and concentration fields appreciably. This is confirmed by comparing the temperature and concentration fields of Fig. 7 with the corresponding ones in Fig. 4. The concentration and velocity profiles along the axis of symmetry (ampoule centerline) are presented in Figs. 6 and 8, respectively. The solutal boundary layer at the growth interface is very thin and extends only about 0.0075 m into the melt, as depicted in Fig. 6. The velocity boundary layers around the void are shown in Fig. 8 for several different void–interface locations. Note that for the $l = 0.0456$ m case, the flow dies long before it penetrates the solutal boundary layer. As a result, at $l = 0.0456$ m, the solidification process is unaffected by the void-generated convection. The radial concentration profile along the growth interface, for this case and several other void–interface distances, is included in Fig. 9. The $l = 0.0456$ m concentration profile is parabolic with the maximum dopant concentration occurring in the middle of the interface. This indicates an appreciable amount of radial segregation, which is mainly caused by the interface curvature.

If the distance between the void and the growth interface is reduced, the interfacial segregation pattern changes drastically, as shown in Fig. 9. That is, as l decreases, the dopant concentration rapidly decreases in the center of the interface and gradually increases near the ampoule wall. Consequently, the dopant concentration distribution observed for the $l = 0.0456$ m case is completely reversed for the $l = 0.033$ m case, where the maximum solutal concentration occurs near the ampoule wall. This can be explained by examining the temperature, concentration, and flowfields included in Fig. 10 for $l = 0.033$ m. In this case, the flow generated by the thermocapillary vortex, shown in Fig. 10a, gets very close to the growth interface. This clockwise recirculating vortex brings the fluid from the upper regions of the ampoule, which is at the low bulk concentration C_0 along the ampoule centerline, and toward the interface. It also carries the higher concentration fluid from the wall–interface region away from the solutal boundary layer and toward upper regions of the ampoule. As a result, this recirculation causes a dip in the solutal boundary layer at the growth interface, which is indicated by the depression of the concentration contours as shown in Fig. 10c.

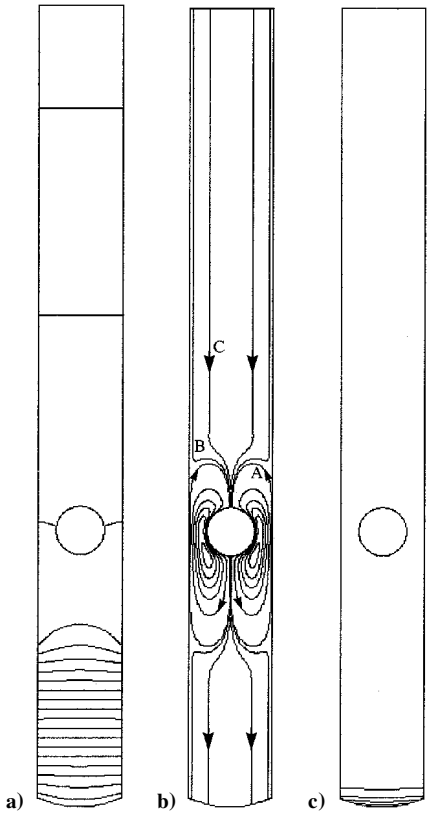

Fig. 7 Case $l = 0.0456$ m: a) temperature field (20 contours, T_{min} = 1238°C and T_{max} = 1264°C), b) streamlines [5 contours on the main vortex with $\psi_{min} = -0.0746(10)^{-2}$ m²/s and $\psi_{max} = 0.24(10)^{-9}$ m²/s, $C = -0.83(10)^{-6}$ m²/s, $B = -0.25(10)^{-5}$ m²/s, and $A = -0.417(10)^{-5}$ m²/s], and c) concentration field (5 contours, $C_{min} = 1.0$ and $C_{max} = 21.6$).

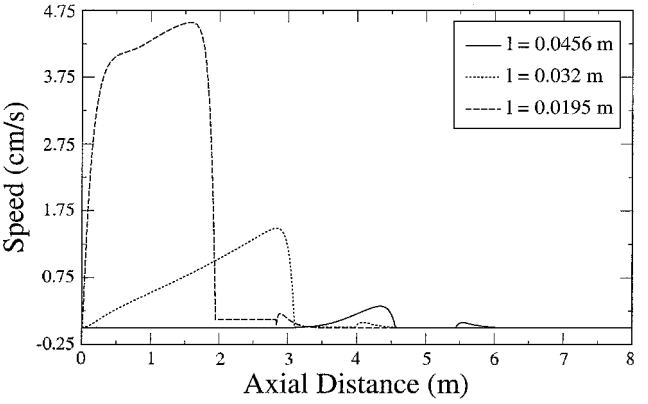

Fig. 8 Speed along the central axis of symmetry for different void–interface distances.

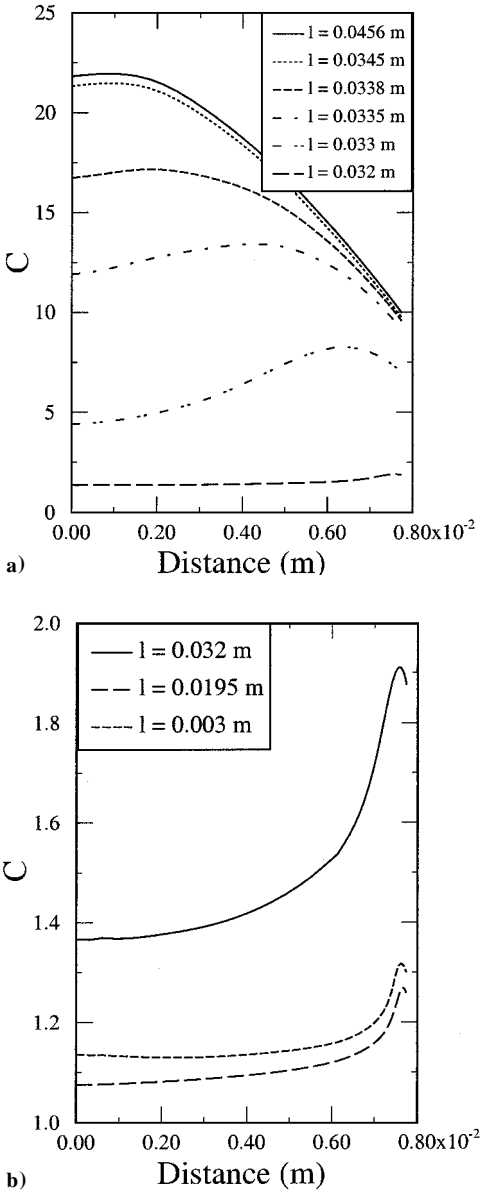

Fig. 9 Concentration as a function of the distance along the solid–melt interface for different void–interface distances.

The flow, temperature, and concentration fields for the $l = 0.032$ m case are included in Fig. 11. In this case, the thermocapillary vortex shown in Fig. 11b has penetrated the solutal buildup region near the growth interface. This is corroborated by an examination of the velocity profile along the ampoule centerline in Fig. 8, which shows that the velocity boundary layer for this case extends all of the way to the growth interface. The strong thermocapillary vortex nearly wipes out the solute boundary layer at the growth interface, as indicated in Figs. 9 and 11c, and homogenizes the dopant concentration throughout the ampoule through vigorous mixing. The $l = 0.032$ m axial and radial concentration profiles included in Figs. 6 and 9a are both indicative of an almost fully mixed regime. However, a closer look at the radial segregation pattern on an expanded scale, as shown in Fig. 9b, still indicates a noticeable nonuniformity in the interfacial concentration profile.

The thermocapillary mixing effect becomes even more pronounced as the void and the interface get closer to each other. At $l = 0.0195$ m the void is in the high-temperature gradient region. Consequently, the thermocapillary flow intensifies with an almost fivefold increase in the velocity as shown in Fig. 8. Comparison of the streamline contours of Fig. 12a with those of Fig. 11a for the $l = 0.032$ m case indicates that the center of the thermocapillary vortex shifts position and moves next to the growth interface. This is

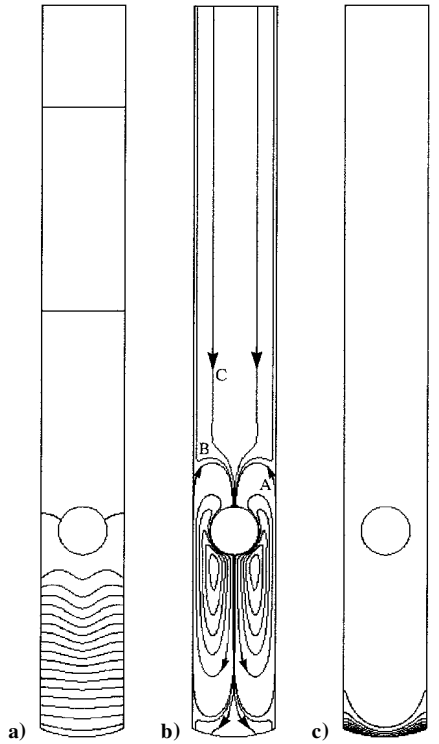

Fig. 10 Case $l = 0.033$ m: a) temperature field (20 contours, T_{min} = 1238°C and T_{max} = 1263.6°C), b) streamlines [5 contours on the main vortex with $\psi_{min} = -0.1466(10)^{-2}$ m²/s and $\psi_{max} = 0.90(10)^{-9}$ m²/s, $C = -0.83(10)^{-6}$ m²/s, $B = -0.25(10)^{-5}$ m²/s, and $A = -0.417(10)^{-5}$ m²/s], and c) concentration field (10 contours, $C_{min} = 1.0$ and C_{max} = 8.26).

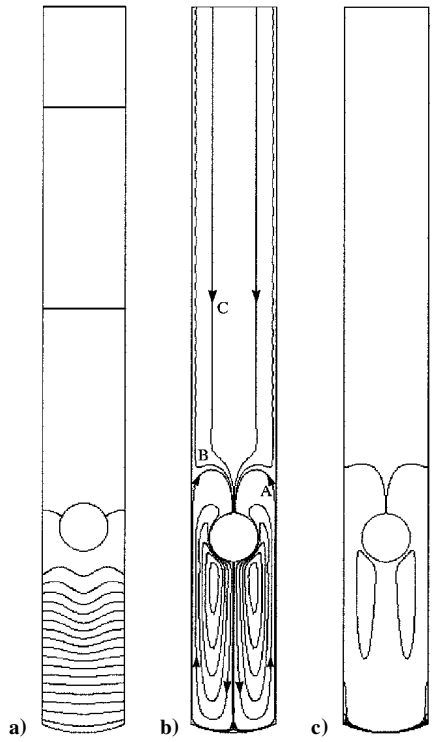

Fig. 11 Case $l = 0.032$ m: a) temperature field (20 contours, T_{min} = 1238°C and T_{max} = 1263.5°C), b) streamlines [5 contours on the main vortex with $\psi_{min} = -0.1427(10)^{-2}$ m²/s and $\psi_{max} = 0.85(10)^{-9}$ m²/s, $C = -0.83(10)^{-6}$ m²/s, $B = -0.25(10)^{-5}$ m²/s, and $A = -0.417(10)^{-5}$ m²/s], and c) concentration field (5 contours, $C_{min} = 1.0$ and C_{max} = 1.91).

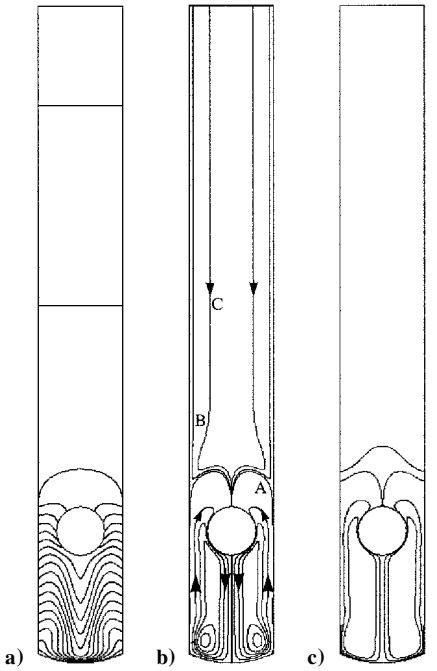

Fig. 12 Case $l = 0.0195$ m: a) temperature field (20 contours, T_{min} = 1238°C and T_{max} = 1263°C), b) streamlines [5 contours on the main vortex with $\psi_{min} = -0.826(10)^{-2}$ m²/s and $\psi_{max} = 0.52(10)^{-6}$ m²/s, $C = -0.83(10)^{-6}$ m²/s, $B = -0.25(10)^{-5}$ m²/s, and $A = -0.417(10)^{-5}$ m²/s], and c) concentration field (10 contours, $C_{min} = 1.0$ and $C_{max} = 1.27$).

because, unlike the flowfields of the earlier cases, which died down before impinging on the interface, in this case the thermocapillary flow is strong enough to reach the solid surface with considerable velocity. This flow must turn rapidly to accommodate the presence of the solid interface. Consequently, the center of the vortex shifts to near the interface region where the maximum vorticity is generated. This also creates a substantial amount of mixing near the interface as indicated by the nearly uniform interfacial concentration profile of Fig. 9b and the concentration, temperature, and flowfields included in Fig. 12. In this case, even the temperature field is significantly affected by the void-generated flow. The drastic distortions of the temperature contours near the interface implies that the flow will now play a dominant role in the interfacial energy balance. Therefore, the assumption of a fixed or empirically derived interface shape and position as adopted in the present analysis becomes highly questionable for this case.

Finally, the temperature, concentration, and flowfields for the $l = 0.003$ m case are presented in Fig. 13. The thermocapillary vortex is now compressed between the void and the growth interface. This slightly decreases the intensity of flow and the extent of mixing. As a result, the radial concentration profile shown in Fig. 9b for this case is slightly more nonuniform than the preceding $l = 0.0195$ m profile.

The results of this analysis can be succinctly summarized by plotting the magnitude of the radial segregation against the void–interface distance as shown in Fig. 14. From a transport point of view, there are three distinct regions on this plot. Points A–B correspond to the region where the solutal boundary layer is minimally affected by the void-generated thermocapillary convection. The segregation behavior in this region is dominated by diffusion and is caused almost entirely by the interface curvature. Points B–C designate a region where the thermocapillary flow begins to influence the segregation pattern considerably (see Fig. 9a), but has not yet penetrated the solutal boundary layer at the growth interface. In this region, the extent of the radial segregation and the distribution of the interfacial composition change drastically with small variations in the void–interface distance. Finally, the segment bounded by points C–D corresponds to the region where the vigorous thermocapillary flow wipes out the solutal boundary layer and a fully mixed regime is approached.

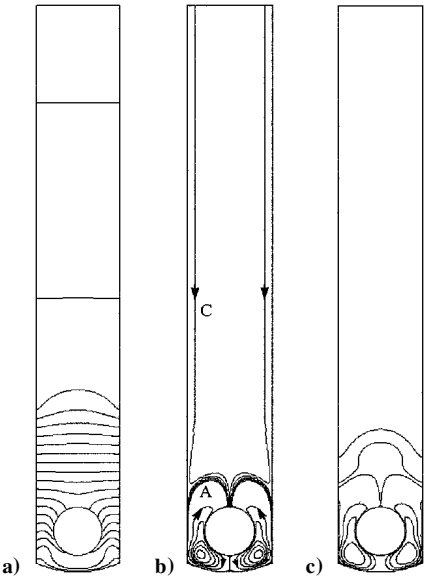

Fig. 13 Case $l = 0.003$ m: a) temperature field (20 contours, T_{min} = 1238°C and T_{max} = 1262.5°C), b) streamlines [5 contours on the main vortex with $\psi_{min} = -0.93(10)^{-2}$ m²/s and $\psi_{max} = 0.27(10)^{-5}$ m²/s and 5 contours between $A = -0.18(10)^{-4}$ m²/s and $C = -0.2(10)^{-5}$ m²/s], and c) concentration field (10 contours, $C_{min} = 1.0$ and $C_{max} = 1.32$).

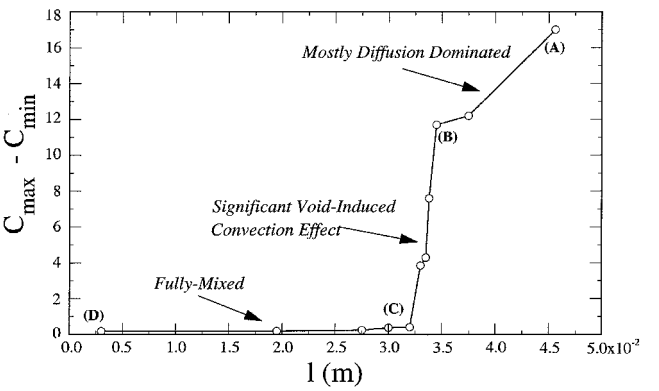

Fig. 14 Radial segregation as a function of the void–interface distance.

Conclusions

Recent microgravity experiments have been hampered by convection caused by unwanted voids and/or bubbles in the melt. In this work, we presented a numerical study to delineate the influence of void-generated thermocapillary convection on the microgravity solidification of a doped single crystal from a dilute binary melt. Through a quasi-steady analysis in which the distance between the void and the solidification interface was kept fixed during each simulation, it was shown that void-generated convection can affect radial solutal segregation drastically, especially if the thermocapillary vortex penetrates the solutal boundary layer at the growth interface. Three different regimes were identified based on the distance between the void and the growth interface. According to this designation, when the void is relatively far from the interface, a diffusion-controlled regime prevails where most of the radial nonuniformity in the interfacial composition is due to interface curvature with minimal flow effects. When the void is relatively close to the interface, a fully mixed regime prevails due to the penetration of the solutal boundary layer by the thermocapillary vortex, which tends to homogenize the interfacial composition. These two regimes are separated by an intermediate region where the radial interfacial concentration changes drastically with the void–interface distance. Naturally, the extent of each of these regions will depend strongly on the material, physical, and growth properties of the system under consideration.

The trends predicted by the model suggest that in the absence of any other relevant driving mechanism for convection in microgravity, the mixing that occurred in melt of the growing crystals during the recent microgravity solidification experiments could be plausibly caused by the voids that evolved in the melt and were detected during the postflight characterization of the samples. The effects of void generated convection can prove to be quite important in designing future microgravity solidification and physical property measurement experiments. Therefore, further direct comparisons between numerical predictions and controlled experimental measurements are needed to confirm the validity of the present conclusions. Extension of the present model is underway to allow transient simulation of the entire solidification process from end to end with free bubble motion.

Acknowledgments

The authors wish to gratefully acknowledge the support provided by the Computational Microgravity Laboratory. This work was supported by NASA Microgravity Science and Applications under Grant NAG-8-1472. The time and effort spent by Emily Nelson in reviewing this manuscript is greatly appreciated.

References

[1]Matthiesen, D. H., and Majewski, J. A., "The Study of Dopant Segregation Behavior During the Growth of GaAs in Microgravity," *Joint Launch + One Year Review of USML-1 and USMP-1*, NASA CP 3272, Vol. 1, 1994, p. 223.

[2]Andrews, J. B., Hayes, L. J., Arikawa, Y., and Coriell, S. R., "Microgravity Solidification of Al–In Alloys," AIAA Paper 97-1012, 1997.

[3]Fripp, A. L., Debnam, W. J., Woodell, G. A., Rosch, W. R., and Narayanan, R., "Effect of Microgravity Direction on the Growth of PbSnTe," AIAA Paper 97-0676, 1997.

[4]Papazian, J. M., and Wilcox, W. R., "Interaction of Bubbles with Solidification Interfaces," *AIAA Journal*, Vol. 16, 1978, pp. 447–451.

[5]Naumann, R., "Marangoni Convection Around Voids in Bridgman Growth," *Journal of Crystal Growth*, Vol. 154, 1995, pp. 156–162.

[6]Wozniak, G., Wozniak, K., and Bergelt, H., "On the Influence of Buoyancy on the Surface Tension Driven Flow Around a Bubble on a Heated Wall," *Experiments in Fluids*, Vol. 21, 1996, pp. 181–186.

[7]Kassemi, M., and Rashidnia, N., "Steady and Oscillatory Thermocapillary Flows Generated by a Bubble in 1-*g* and Low-*g* Environments," AIAA Paper 97-0924, 1997.

[8]Kassemi, M., and Rashidnia, N., "Oscillatory and Steady Thermocapillary and Natural Convective Flows Generated by a Bubble: Numerical–Experimental Comparisons," *Proceedings of the Joint Xth European and Russian Symposium on Physical Sciences in Microgravity*, edited by V. S. Avdyevsky and V. I. Polezhaev, Vol. 1, Russian Academy of Sciences, St. Petersburg, 1997, pp. 110–117.

[9]Kassemi, M., Rashidnia, N., and Mercer, C., "Numerical and Experimental Visualization of Oscillatory Temperature and Velocity Fields Generated by a Bubble," *Proceedings of the 8th International Symposium in Flow Visualization*, edited by G. M. Carlomagno and I. Grant, Univ. of Edinburgh, Edinburgh, 1998, pp. 284.1–284.11.

[10]Shetty, R., Balasubramanian, R., and Wilcox, R., "Surface Tension and Contact Angle of Molten Semiconductor Compounds II. Gallium Arsenide," *Journal of Crystal Growth*, Vol. 100, 1990, pp. 58–62.

[11]Kassemi, M., and Rashidnia, N., "Steady and Oscillatory Thermocapillary Convection Generated by a Bubble," *Physics of Fluids*, Vol. 12, No. 12, 2000.

[12]Kaforey, M. L., Bly, J. M., and Matthiesen, D. H., "Void Formation in Gallium Arsenide Crystals Grown in Microgravity," *Journal of Crystal Growth*, Vol. 174, 1997, pp. 112–119.

[13]Coriell, S., and Sekerka, R., "Lateral Solute Segregation During Unidirectional Solidification of a Binary Alloy with Curved Solid–Liquid Interface," *Journal of Crystal Growth*, Vol. 46, 1979, p. 479.